The Journal of Chemical Physics

RESEARCH ARTICLE | JUNE 22 2023

High resolution electronic spectroscopy of uranium mononitride, UN

Anh T. Le; Xi-lin Bai; Michael C. Heaven ; Timothy C. Steimle

J. Chem. Phys. 158, 244301 (2023)
https://doi.org/10.1063/5.0157884
CHORUS

AIP Publishing

The Journal of Chemical Physics ARTICLE scitation.org/journal/jcp

High resolution electronic spectroscopy of uranium mononitride, UN

Cite as: J. Chem. Phys. 158, 244301 (2023); doi: 10.1063/5.0157884
Submitted: 12 May 2023 • Accepted: 5 June 2023 •
Published Online: 22 June 2023

Anh T. Le,[1] Xi-lin Bai,[2] Michael C. Heaven,[3,a)] and Timothy C. Steimle[4]

AFFILIATIONS

[1] School of Chemistry and Biochemistry, Georgia Institute of Technology, Atlanta, Georgia 30318, USA
[2] School of Physics and Information Engineering, Key Laboratory of Spectral Measurement and Analysis of Shanxi Province, Shanxi Normal University, Linfen 041004, China
[3] Department of Chemistry, Emory University, Atlanta, Georgia 30322, USA
[4] School of Molecular Sciences, Arizona State University, Tempe, Arizona 85287, USA

[a)] **Author to whom correspondence should be addressed:** mheaven@emory.edu. **Telephone:** 404 727 6617.

ABSTRACT

The isoelectronic molecules UN and UO^+ are known to have Ω = 3.5 and Ω = 4.5 ground states, respectively (where Ω is the unsigned projection of the electronic angular momentum along the internuclear axis). A ligand field theory model has been proposed to account for the difference [Matthew and Morse, J. Chem. Phys. 138, 184303 (2013)]. The ground state of UO^+ arises from the $U^{3+}(5f^3(^4I_{4.5}))O^{2-}$ configuration. Owing to the higher nominal charge of the N^{3-} ligand, the U^{3+} ion in UN is stabilized by promoting one of the 5*f* electrons to the more polarizable 7*s* orbital, reducing the repulsive interaction with the ligand and rendering $U^{3+}(5f^27s(^4H_{3.5}))N^{3-}$ the lowest energy configuration. In the present work, we have advanced the characterization of the UN ground state through studies of two electronic transitions, [18.35]4.5-*X*(1)3.5 and [18.63]4.5-*X*(1)3.5, using sub-Doppler laser excitation techniques with fluorescence detection. Spectra were recorded under field-free conditions and in the presence of static electric or magnetic fields. The ground state electric dipole moment [μ = 4.30(2) D] and magnetic g_e-factor [2.160(9)] were determined from these data. These values were both consistent with the $5f^27s$ configurational assignment. Dispersed fluorescence measurements were used to determine vibrational constants for the ground and first electronically excited states. Electric dipole moments and magnetic g_e-factors are also reported for the higher-energy electronically excited states.

INTRODUCTION

The electronic structure of gas-phase UN has attracted attention, in part due to the interesting contrast with isoelectronic UO^+. Previous studies[1–3] have shown that the ground state of UO^+ arises from the formal configuration $U^{3+}(5f^3)O^{2-}$. The 5*f* electrons retain much of their atomic character, with the lowest energy distribution corresponding to the $5f^3\,^4I_{4.5}$ atomic ion state.[1] The electronic angular momentum (J_a = 4.5) is then quantized relative to the internuclear axis, producing states with Ω (the unsigned projection of J_a along the bond axis) = 4.5, 3.5, 2.5, 1.5, and 0.5, in ascending energy order. Hence, the electronic ground state is the Ω = 4.5 component. This pattern of energy levels is consistent with a ligand field theory (LFT) model of the low-energy electronic structure.[1]

Given this background, it was surprising when Matthew and Morse[2] discovered an Ω = 3.5 ground state for UN. Using an LFT model, they argued that the ground state was derived from the $U^{3+}(5f^27s)N^{3-}$ configuration. The difference, as compared to UO^+, was attributed to the greater charge of the N^{3-} ligand. This destabilizes the U 5*f* orbitals relative to the more polarizable 7*s* orbital, to the extent that the $5f^27s$ configuration becomes energetically favored. This model was subsequently supported by high-level relativistic quantum chemistry calculations for UN (inclusive of spin–orbit coupling). The studies of Battey *et al.*[4] and de Melo *et al.*[5] yielded Ω = 3.5 ground state wavefunctions that had $5f^27s$ fractional characters of 84% and 83%, respectively. Both studies also reported the molecular constants for many low-energy electronic states: 27 states below 10 000 cm^{-1} (Ref. 4) and 62 states below 20 000 cm^{-1} (Ref. 5).

Matthew and Morse[2] examined the electronic transitions of UN in the spectral range from 19 200 to 23 900 cm^{-1} using mass-selected resonant two-photon (R2PI) ionization spectroscopy. They

observed numerous bands, of which seven were investigated at the level of rotational resolution with the [18.35]4.5 ← $X(1)3.5$ band near 18 349 cm^{-1} being most relevant to the present study. Battey *et al.*[4] also performed mass-selected R2PI spectroscopy as part of their experimental and theoretical effort to determine the ionization energy of UN. They detected and rotationally resolved the [18.63]4.5 ← $X(1)3.5$ band near 18 633 cm^{-1}. More recently, de Melo *et al.*[5] probed low energy electronic states of UN by means of UN^- anion photo-detachment spectroscopy. The threshold detachment peak defined an electron affinity for UN of 1.4 eV, and a cluster of excited states was evident, starting at an energy that was ~0.6 eV above the ground state of UN. The congested structure of the photo-detachment spectrum was analyzed through comparison with the predictions of high-level electronic structure calculations.[5] The only other spectroscopic data available for UN were obtained by Green and Reedy,[6] who observed site dependent fundamental vibrational intervals of 1000.9, 995.5, and 991.9 cm^{-1} for matrix isolated UN.

Limited spectroscopic data are available for UN^+. Battey *et al.*[4] used two-color pulsed field ionization-zero kinetic (PFI-ZEKE) photoelectron spectroscopy to determine the UN ionization energy (6.2987 eV), UN^+ ground state Ω value (=4), and the vibrational interval (1072 cm^{-1}). The Ω = 4 value was consistent with the expectation that the first ionization limit would correspond to the removal of the 7*s* electron.

In the present study, we have used high-resolution electronic spectroscopy with laser-induced fluorescence (LIF) detection to examine the electric dipole moment and magnetic g_e-factor for the [18.63]4.5, [18.35]4.5, and $X(1)3.5$ states of UN. For the ground state, the electric dipole moment is a particularly good benchmark for testing the predictions of relativistic electronic structure calculations.[7] Further insights concerning the parent electronic configuration for the ground and excited electronic states are derived from an analysis of the magnetic g_e-factors. As these measurements were conducted at a spectral resolution significantly higher than the previous R2PI measurments[2,4] (a full-width at half maximum of ~40 MHz as compared to ~6 GHz), we also report improved field-free molecular constants for the [18.63]4.5, [18.35]4.5, and $X(1)3.5$ states. Finally, medium spectral resolution LIF spectroscopy was used to record the two-dimensional (2-D) (excitation and dispersed LIF) spectra. These measurements yielded the identification of the [0.47]4.5 low-lying excited state and the determination of the [0.47]4.5 and $X(1)3.5$ vibrational intervals.

EXPERIMENTAL

The method used for the production of a cold (rotational temperature ~ 10 K) supersonic molecular sample of UN was similar to that used in our previous studies of UO[8] and UF.[9] Specifically, UN was generated via 532 nm laser ablation of a depleted uranium rod in the presence of a pulsed supersonic expansion of a 5% NH_3/95% argon mixture. Low-spectral resolution laser excitation survey spectral scans were recorded using a pulsed dye laser, probing a free-jet expansion of ~10 cm downstream from the nozzle orifice. In the case of the high-resolution field-free, Stark and Zeeman measurements, the free-jet expansion was skimmed and the resulting collimated molecular beam probed ~50 cm from the source. Laser-induced fluorescence (LIF) detection was used in both the high-resolution and low-resolution measurements.

The initial detection and characterization of UN were achieved using a two-dimensional (2-D) technique previously described.[10–12] In this approach, the LIF is wavelength dispersed horizontally across the two-dimensional gated and intensified charge coupled device (ICCD) array, which is attached to the exit port of a 0.67 m monochromator. The camera software sums down the vertical arrays of the ICCD and returns a one-dimensional array of intensity vs dispersed fluorescence wavelength for a given laser excitation wavelength. The laser wavelength is then stepped, and the process is repeated, to produce a 2-D spectrum with one of the dimensions being the laser excitation wavelength and the other dimension being the dispersed fluorescence (DF). In the visible range, an ~75 nm window of the DF spectrum is viewed at a given laser excitation. Typically, the entrance slits of the monochromator were set to produce a spectral resolution of ~0.7 nm, the signal from 20 ablation pulses was summed, and the pulsed dye laser was stepped in 0.1 cm^{-1} increments.

The high-resolution field-free, Stark and Zeeman spectra were recorded using the spectrometer described in the previous investigations of UO[8] and UF.[9] The excitation radiation was generated by a single-mode, continuous wave (CW) ring dye laser. The absolute wavelength was calibrated by co-recording the sub-Doppler I_2 spectrum[13] and the relative wavelength by co-recording the transmission of an actively stabilized confocal etalon. Static electric fields were generated by the application of a voltage across a pair of highly transmitting, conducting neutral density filters. The field strength was calibrated by means of a voltmeter and mechanical measurement of the plate separation. For the Zeeman measurements, homogeneous magnetic fields were generated by a pair of rare earth magnets attached to an iron yoke. The molecular beam passed through 5.0 mm holes in the center of the magnet/yoke assembly. The field was calibrated using a commercial gauss meter. A polarization rotator was used to align the electric field vector of the linearly polarized laser light relative to the static magnetic or electric fields. Systematic errors of up to 2% are estimated for both the static electric and magnetic field strengths.

Field-free measurements

The two electronic transitions examined in this study, [18.35]4.5-$X(1)3.5$ and [18.63]Ω- $X(1)3.5$, had both been observed in earlier mass-selected R2PI experiments using pulsed dye laser excitation.[2,4] We extended the characterization of these transitions by recording 2-D fluorescence excitation spectra. Figure 1 shows the result for excitation wavelengths that cover the range of the [18.63]Ω- $X(1)3.5$ origin band. The horizontal axis gives the photon energy of the excitation laser, and the vertical axis gives the difference between the energies of the emitted and exciting photons. The trace at the bottom of Fig. 1 shows the 1-D LIF spectrum obtained by summing the fluorescence intensities within the dashed-line box that is centered at zero energy offset (i.e., on-resonance). The vertical trace at the far right-hand side of the figure shows the 1-D dispersed fluorescence spectrum obtained by summing the fluorescence intensities contained in the dashed-line box that is centered at an excitation energy of 18 635 cm^{-1}. An expanded version of the LIF trace is shown in Fig. 2, along with a simulation generated using the PGOPHER software package.[14] The resolution of Fig. 2 is significantly better than the corresponding Fig. 1 of Ref. 4. In the earlier

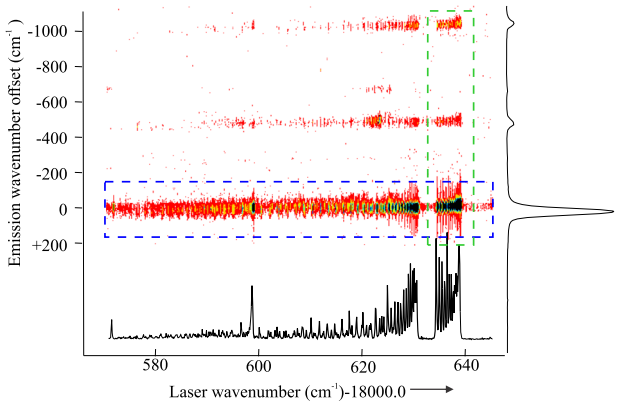

FIG. 1. The 2-D spectrum of the products of an ablated U/NH_3 supersonic expansion in the 18 570–18 645 cm^{-1} spectral range. The horizontal axis is the laser excitation wavenumber, and the vertical axis is the dispersed laser-induced fluorescence (DF) wavenumber relative to the laser excitation. The spectral window of the DF is tracked with the laser excitation wavenumber. At the bottom is the medium resolution $X(1)3.5 \rightarrow$ [18.63]4.5 LIF excitation spectrum obtained by the vertical integration of the indicated horizontal slice centered on the laser wavenumber (i.e., on-resonance detection). On the right is the DF spectrum obtained by horizontal integration of the indicated vertical rectangular slice centered at the [18.63]4.5-$X(1)3.5$ bandhead (ν = 18 635 cm^{-1}).

study, the upper state Ω value was tentatively assigned as Ω = 3.5, but the quality of the data was not sufficient to rule out the possibility of Ω = 4.5. Figure 2 and the high-resolution spectra definitively confirmed that the upper state is Ω = 4.5 [the Q(3.5) and P(4.5) lines were not present in the high-resolution spectra]. An error in the band origin previously reported for the [18.63]Ω-$X(1)3.5$ transition was also discovered. In re-examining the earlier data, we found that the uncalibrated wavenumber scale provided by the dye laser scanning program had been inadvertently used for both the display of

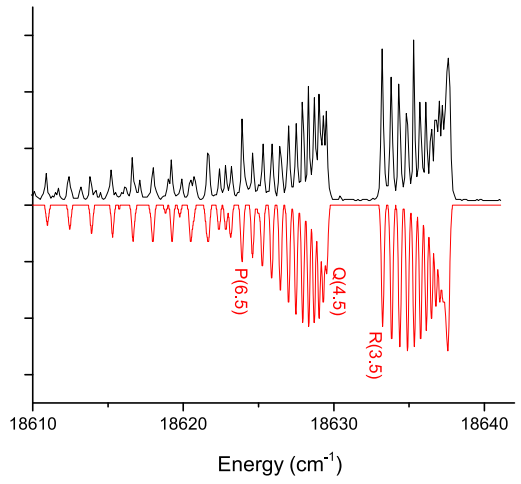

FIG. 2. Rotationally resolved LIF spectrum of the UN [18.63]4.5-$X(1)3.5$ 0-0 transition. The downward-going trace is a simulation generated using the PGOPHER software package. The rotational temperature for this simulation was 70 K.

this band (Fig. 1 of Ref. 4) and the fitting of the molecular constants. Hence, the T_0 value reported here (18 630.064 cm^{-1}) supersedes the earlier determination, which was in error by +5.6 cm^{-1}. Note that we are using corrected labeling for this state as it was formerly designated as [18.64]3.5.

A 2-D spectrum in the vicinity of the [18.35]4.5-$X(1)3.5$ transition is shown in Fig. 3. The trace at the bottom shows the 1-D LIF spectrum obtained by summing the fluorescence intensities within the dashed-line box that is centered at zero energy offset and exhibits the intense [18.35]4.5-$X(1)3.5$ band, as well as a weaker band with a red degraded bandhead near 18 400 cm^{-1}. The latter is assigned as the [18.40]-$X(1)3.5$ transition (see below) of UN. Note that the [18.338]3-$X(1)4$ band[2] of background UO, which has an R-branch head near 18 355 cm^{-1}, overlapped the [18.35]4.5-$X(1)3.5$ band of UN. Fortunately, the [18.338]3 state of UO preferentially fluoresces off-resonant, whereas the [18.35]4.5 state of UN preferentially fluoresces on-resonant upon excitation, causing the 1-D LIF spectrum to be dominated by UN spectral features. The vertical traces marked "A–C" on the far right-hand side of Fig. 3 show the 1-D dispersed fluorescence spectra obtained by summing the fluorescence intensities contained in the dashed-line boxes centered at excitation energies of 18 345 cm^{-1} (box "A"), 18 355 cm^{-1} (box "B"), and 18 400 cm^{-1} (box "C"). DF spectrum "A" is dominated by off-resonance UO emission. DF spectrum "B" is predominately the on-resonance UN emission, while DF spectrum "C" exhibits both on-resonance and off-resonance UN emission. Evidently, the vibronic wavefunction for the [18.35]4.5 and [18.40] states of UN are significantly different causing the Franck–Condon factor for the [18.35]4.5-$X(1)3.5$ transition to be near unity (i.e., diagonal) and that for the [18.40]-$X(1)3.5$ transition to be significantly non-diagonal.

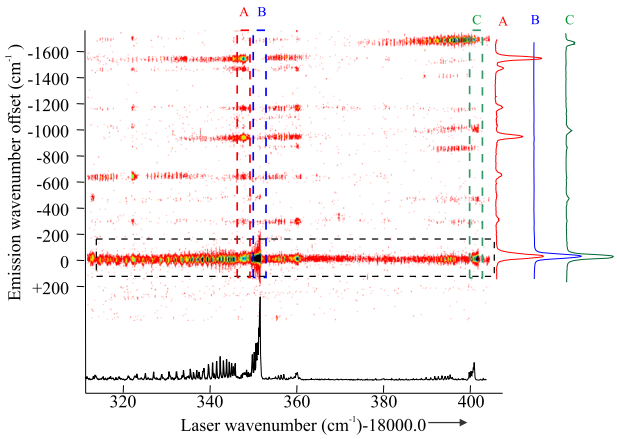

FIG. 3. The 2-D spectrum of the products of an ablated U/NH_3 supersonic expansion in the 18 310 to 18 405 cm^{-1} spectral range. At the bottom is the medium resolution excitation spectrum obtained by vertical integration of the indicated horizontal slice centered on the laser wavenumber (i.e., on-resonance detection), which is dominated by the [18.35]4.5-$X(1)3.5$ and the weaker [18.40]-$X(1)3.5$ bands of UN. On the right are the DF spectra obtained by the horizontal integration of the indicated vertical rectangular slice centered at the [18.35]4.5-$X(1)3.5$ bandhead (ν = 18 355 cm^{-1}), a weaker band head at 18 345 cm^{-1}, which is assigned as the [18.338]3-$X(1)4$ band of UO (Mathew and Morse[2]) and the bandhead near 18 400 cm^{-1}.

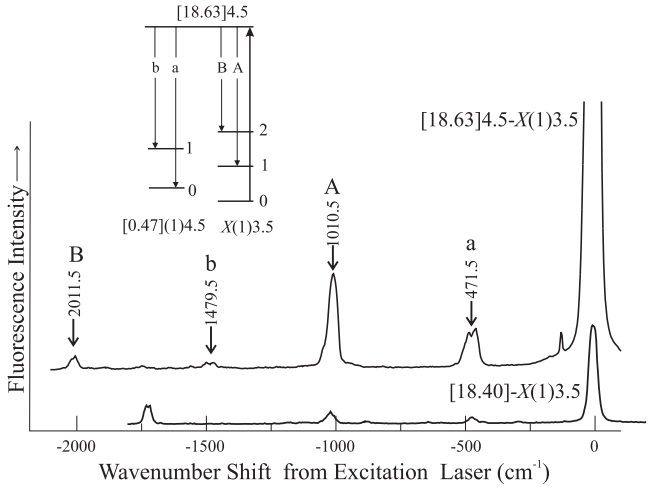

FIG. 4. The DF spectra extracted from the 2-D spectra in the region of R-branch heads of the [18.63]4.5-*X*(1)3.5 and weaker [18.40]-*X*(1)3.5 bands of UN. The inset shows the associated energy level diagram and assignment. The numbers above the peaks are the Stokes shifts in wavenumbers. The Stokes shifts of "A" and "a" features for the two bands are identical, supporting the assignment of the [18.40]-*X*(1)3.5 band.

TABLE II. Molecular constants for the *X*(1)3.5($v'' = 0$), [18.35]4.5, and [18.63]4.5 states of UN. cm^{-1} units except for the dipole moments and the dimensionless *g*-factors.

Parameter	X(1)3.5($v'' = 0$)	[18.35]4.5	[18.63]4.5
B	0.40948(9)	0.3766(1)	0.38864(8)
$10^7 D$	10(7)	69(9)	17(6)
$\lvert\vec{\mu}_{el}\rvert$ (D)	4.30(2)	4.05(3)	4.32(2)
g-factor	2.160(9)	3.93(1)	3.599(9)
T_0	0	18 349.289(3)	18 630.064(1)

The DF spectra extracted from the 2-D spectra in the region of R-branch heads of the [18.63]4.5-*X*(1)3.5 and weaker [18.40]-*X*(1)3.5 bands of UN are shown in Fig. 4. Also shown is the associated energy level diagram, with relevant assignments, for the DF spectrum for the [18.63]4.5-*X*(1)3.5 bandhead excitation. That DF spectrum exhibits emission at the $v'' = 0$, 1, and 2 levels of the *X*(1)3.5 state and the $v'' = 0$ and 1 levels of the [0.47](1)4.5 state. The measured $\Delta G_{1/2}$ and $\Delta G_{3/2}$ vibrational spacings for the *X*(1)3.5 state are 1010.5 ± 5.0 and 1001.0 ± 5.0 cm^{-1}, respectively. These energy spacings yield the vibrational constants ω_e = 1020 and

TABLE I. Observed and calculated line positions (cm^{-1}) of the [18.35]4.5-*X*(1)3.5($v'' = 0$) and [18.63]4.5-*X*(1)3.5($v = 0$) bands of UN [18.35]4.5- *X*(1)3.5($v'' = 0$) and [18.63]4.5-*X*(1)3.5($v'' = 0$).

[18.35]4.5-*X*(1)3.5($v'' = 0$)					[18.63]4.5-*X*(1)3.5($v'' = 0$)				
Line	J'	J''	Observed[a]	Obs-Calc	Line	J'	J''	Observed[b]	Obs-Calc
R(3.5)	4.5	3.5	52.1570	−0.0007	*R*(3.5)	4.5	3.5	33.2344	0.0013
R(4.5)	5.5	4.5	52.6091	−0.0023	*R*(4.5)	5.5	4.5	33.8232	0.0013
R(5.5)	6.5	5.5	52.9961	−0.0006	*R*(5.5)	6.5	5.5	34.3707	0.0021
R(6.5)	7.5	6.5	53.3114	−0.0013	*R*(6.5)	7.5	6.5	34.8730	−0.0001
R(7.5)	8.5	7.5	53.5569	−0.0013	*R*(7.5)	8.5	7.5	35.3363	0.0011
R(8.5)	9.5	8.5	53.7335	0.0013	*R*(8.5)	9.5	8.5	35.7549	0.0001
Q(4.5)	4.5	4.5	48.4716	−0.0009	*R*(9.5)	10.5	9.5	36.1325	0.0008
Q(5.5)	5.5	5.5	48.1081	0.0006	*R*(10.5)	11.5	10.5	36.4634	−0.0023
Q(6.5)	6.5	6.5	47.6753	0.001	*R*(11.5)	12.5	11.5	36.7559	−0.0007
Q(7.5)	7.5	7.5	47.1732	0.0012	*R*(12.5)	13.5	12.5	37.0046	0.0003
Q(8.5)	8.5	8.5	46.5986	−0.0008	*R*(13.5)	14.5	13.5	37.2093	0.0007
Q(9.5)	9.5	9.5	45.9561	0.0006	*Q*(4.5)	4.5	4.5	29.5463	−0.0016
Q(10.5)	10.5	10.5	45.2386	−0.0003	*Q*(5.5)	5.5	5.5	29.3185	0.0005
P(5.5)	4.5	5.5	43.9693	0.0007	*Q*(6.5)	6.5	6.5	29.0475	0.0012
P(6.5)	5.5	6.5	42.7872	0.0021	*Q*(7.5)	7.5	7.5	28.7313	−0.0011
P(7.5)	6.5	7.5	41.5353	0.0017	*Q*(8.5)	8.5	8.5	28.3779	0.0015
P(8.5)	7.5	8.5	40.2127	−0.0004	*Q*(9.5)	9.5	9.5	27.9773	−0.0008
P(9.5)	8.5	9.5	38.8223	−0.0005	*P*(5.5)	4.5	5.5	25.0412	−0.0028
					P(6.5)	5.5	6.5	23.9955	−0.0002
					P(7.5)	6.5	7.5	22.9042	−0.0014
Rms = 0.0012 cm^{-1}					σ = 0.0014 cm^{-1}				

[a]Line centers—18 300 cm^{-1}.
[b]Line centers—18 600 cm^{-1}.

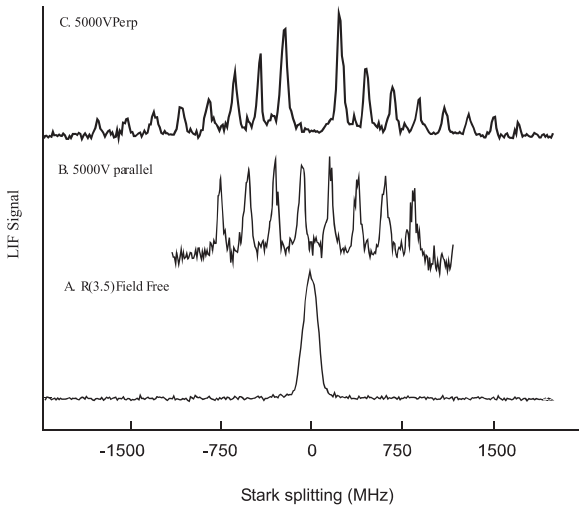

FIG. 5. Stark-effect spectra for the [18.63]4.5-*X*(1)3.5 R(3.5) rotational line. Trace A was recorded under field-free conditions. Traces B and C show the line splittings resulting from the application of an electric field of 2626.8 V/cm.

$\omega_e x_e$ = 4.2 cm^{-1}. The measured $\Delta G_{1/2}$ for the [0.47](1)4.5 state is 1008 ± 5 cm^{-1}. The vibrational shifts in the DF spectrum resulting from the excitation of the [18.40]-*X*(1)3.5 band are identical to those resulting from the excitation of the [18.63]4.5-*X*(1)3.5 band, which is the basis for the assignment. The upper energy state of the band is a new electronic state rather than an excited vibrational level of [18.63]4.5 state. The band 471.5 cm^{-1} below the laser excitation energy is consistent with emission down to the (1)4.5 first electronically excited state. The *ab initio* calculations of Battey *et al.*[4] and de Melo *et al.*[5] predict energies for this state of 441 and 452 cm^{-1}, respectively.

Measurements carried out using the cw-dye laser system achieved an effective resolution of 40 MHz FWHM. As the previous studies of UN were carried out at much lower resolution (around 6 GHz), we recorded the bands of interest at high-resolution, under field-free conditions. The spectra exhibited P, Q, and R lines that spanned the range of excited state rotational levels from J' = 4.5 to 10.5 ([18.35]4.5) and J' = 4.5 to 13.5 ([18.63]4.5). There was no evidence of a measurable Ω-doublet splitting for either transition. The line centers derived from these data are collected in Table I. Molecular constants were obtained by least-squares fitting of the line centers (υ) to the expression

TABLE III. Observed and calculated Stark splittings (MHz) for the R(3.5) line of the UN [18.35]4.5-*X*(1)3.5(v'' = 0) transition.

Line, pol	M_J'	M_J''	Field (V/cm)	Shift (MHz)	Δ (MHz)	Line, pol	M_J'	M_J''	Field (V/cm)	Shift (MHz)	Δ (MHz)
R(3.5)//	3.5	3.5	253.12	−108	−10	*R*(3.5)//	3.5	3.5	3037.97	−1212	−38
	−3.5	−3.5	253.12	100	2		2.5	2.5	3037.97	−859	−21
	3.5	3.5	506.33	−175	21		1.5	1.5	3037.97	−500	3
	2.5	2.5	506.33	−112	28		0.5	0.5	3037.97	−160	8
	1.5	1.5	506.33	− 73	11		−0.5	−0.5	3037.97	186	18
	0.5	0.5	506.33	− 32	−4		−1.5	−1.5	3037.97	528	25
	−0.5	−0.5	506.33	39	11		−2.5	−2.5	3037.97	858	20
	−1.5	−1.5	506.33	86	3		−3.5	−3.5	3037.97	1201	27
	−2.5	−2.5	506.33	131	−9	*R*(3.5)⊥	4.5	3.5	3544.30	−20	39
	−3.5	−3.5	506.33	199	3		−4.5	−3.5	3544.30	20	−39
R(3.5)//	3.5	3.5	1012.66	−390	1		−3.5	−2.5	3544.30	−320	12
	2.5	2.5	1012.66	−278	1		−2.5	−1.5	3544.30	−715	8
	1.5	1.5	1012.66	−169	−2		−1.5	−0.5	3544.30	−1099	16
	0.5	0.5	1012.66	− 51	5		−0.5	0.5	3544.30	−1505	1
	−0.5	−0.5	1012.66	51	−5		0.5	1.5	3544.30	−1920	−22
	−1.5	−1.5	1012.66	173	5		3.5	2.5	3544.30	366	34
	−2.5	−2.5	1012.66	289	9		2.5	1.5	3544.30	757	33
	−3.5	−3.5	1012.66	404	13		1.5	0.5	3544.30	1145	30
R(3.5)//	3.5	3.5	1533.16	−629	−36		0.5	−0.5	3544.30	1504	−2
	2.5	2.5	1533.16	−437	−14						
	1.5	1.5	1533.16	−271	−17						
	0.5	0.5	1533.16	− 76	9						
	−0.5	−0.5	1533.16	103	18						
	−1.5	−1.5	1533.16	281	27						
	−2.5	−2.5	1533.16	453	30						
	−3.5	−3.5	1533.16	630	37						

Rms = 19.36 MHz σ = 20.04 MHz

TABLE IV. Observed and calculated Stark splittings (MHz) for the R(3.5) and Q(4.5) lines of the UN [18.63]4.5-*X*(1)3.5(v'' = 0) transition.

Line, pol	M_J'	M_J''	Field (V/cm)	Shift (MHz)	Δ (MHz)	Line, pol	M_J'	M_J''	Field (V/cm)	Shift (MHz)	Δ (MHz)
R(3.5)⊥	4.5	3.5	1533.16	146	6	*Q*(4.5)//	4.5	4.5	1533.16	636	27
	−4.5	−3.5	1533.16	−133	7		3.5	3.5	1533.16	470	−3
	3.5	2.5	1533.16	305	32		2.5	2.5	1533.16	332	−6
	−3.5	−2.5	1533.16	−279	−6		1.5	1.5	1533.16	194	−9
	2.5	1.5	1533.16	438	33		0.5	0.5	1533.16	46	−22
	−2.5	−1.5	1533.16	−425	−20		−0.5	−0.5	1533.16	−37	31
	1.5	0.5	1533.16	584	46		−1.5	−1.5	1533.16	−221	−18
	−1.5	−0.5	1533.16	−558	−20		−2.5	−2.5	1533.16	−360	−22
	0.5	−0.5	1533.16	730	60		−3.5	−3.5	1533.16	−489	−16
	−0.5	0.5	1533.16	−704	−34		−4.5	−4.5	1533.16	−627	−18
	−0.5	−1.5	1533.16	863	61	Q(4.5)//	4.5	4.5	2626.80	1022	−21
	0.5	1.5	1533.16	−850	−48		3.5	3.5	2626.80	800	−11
	−1.5	−2.5	1533.16	996	61		2.5	2.5	2626.80	563	−16
	1.5	2.5	1533.16	−996	−61		1.5	1.5	2626.80	304	−44
	−2.5	−3.5	1533.16	1142	75		0.5	0.5	2626.80	111	−5
	2.5	3.5	1533.16	−1128	−61		−0.5	−0.5	2626.80	−111	5
R(3.5)⊥	4.5	3.5	2090.10	193	2		−1.5	−1.5	2626.80	−355	−7
	−4.5	−3.5	2090.10	−167	24		−2.5	−2.5	2626.80	−570	9
	3.5	2.5	2090.10	386	14		−3.5	−3.5	2626.80	−800	11
	−3.5	−2.5	2090.10	−348	24		−4.5	−4.5	2626.80	−962	81
	2.5	1.5	2090.10	567	15	Q(4.5)⊥	4.5	3.5	1533.16	1145	68
	−2.5	−1.5	2090.10	−528	24		−4.5	−3.5	1533.16	−1158	−81
	1.5	0.5	2090.10	747	14		3.5	2.5	1533.16	1004	62
	−1.5	−0.5	2090.10	−708	25		−3.5	−2.5	1533.16	−1004	−62
	0.5	−0.5	2090.10	953	40		2.5	1.5	1533.16	849	42
	−0.5	0.5	2090.10	−889	24		−2.5	−1.5	1533.16	−862	−55
	−0.5	−1.5	2090.10	1121	27		1.5	0.5	1533.16	708	37
	0.5	1.5	2090.10	−1082	12		−1.5	−0.5	1533.16	−708	−37
	−1.5	−2.5	2090.10	1301	27		0.5	−0.5	1533.16	553	17
	1.5	2.5	2090.10	−1275	−1		−0.5	0.5	1533.16	−592	−56
	−2.5	−3.5	2090.10	1468	13		−0.5	−1.5	1533.16	425	24
	2.5	3.5	2090.10	−1443	12		0.5	1.5	1533.16	−437	−36
R(3.5)⊥	4.5	3.5	2626.80	241	1		−1.5	−2.5	1533.16	283	17
	−4.5	−3.5	2626.80	−203	37		1.5	2.5	1533.16	−296	−30
	3.5	2.5	2626.80	470	3		−2.5	−3.5	1533.16	142	12
	−3.5	−2.5	2626.80	−406	61		2.5	3.5	1533.16	−142	−12
	2.5	1.5	2626.80	685	−9	Q(4.5)⊥	4.5	3.5	2090.10	1533	65
	−2.5	−1.5	2626.80	−622	72		−4.5	−3.5	2090.10	−1623	−155
	1.5	0.5	2626.80	914	−7		3.5	2.5	2090.10	1240	−44
	−1.5	−0.5	2626.80	−838	83		−3.5	−2.5	2090.10	−1406	−122
	0.5	−0.5	2626.80	1117	−31		2.5	1.5	2090.10	1061	−39
	−0.5	0.5	2626.80	−1079	69		−2.5	−1.5	2090.10	−1201	−101
	−0.5	−1.5	2626.80	1320	−55		1.5	0.5	2090.10	895	−20
	0.5	1.5	2626.80	−1295	80		−1.5	−0.5	2090.10	−984	−69
	−1.5	−2.5	2626.80	1536	−66		0.5	−0.5	2090.10	716	−15
	1.5	2.5	2626.80	−1510	92		−0.5	0.5	2090.10	−792	−61
	−2.5	−3.5	2626.80	1726	−102		−0.5	−1.5	2090.10	536	−10
	2.5	3.5	2626.80	−1764	64		0.5	1.5	2090.10	−588	−42
R(3.5)//	3.5	3.5	1533.16	−432	31		−1.5	−2.5	2090.10	358	−4
	2.5	2.5	1533.16	−301	30		1.5	2.5	2090.10	−383	−21
	1.5	1.5	1533.16	−169	30		−2.5	−3.5	2090.10	192	14

TABLE IV. (*Continued*.)

Line, pol	M_J'	M_J''	Field (V/cm)	Shift (MHz)	Δ (MHz)	Line, pol	M_J'	M_J''	Field (V/cm)	Shift (MHz)	Δ (MHz)
	0.5	0.5	1533.16	−47	19		2.5	3.5	2090.10	−204	−26
	−0.5	−0.5	1533.16	84	18	$Q(4.5)$ ⊥	4.5	3.5	2319.00	1564	−65
	−1.5	−1.5	1533.16	235	36		−4.5	−3.5	2319.00	−1628	1
	−2.5	−2.5	1533.16	348	17		3.5	2.5	2319.00	1359	−66
	−3.5	−3.5	1533.16	488	25		−3.5	−2.5	2319.00	−1410	15
$R(3.5)$//	3.5	3.5	2090.10	−620	12		2.5	1.5	2319.00	1167	−53
	2.5	2.5	2090.10	−451	0		−2.5	−1.5	2319.00	−1205	15
	1.5	1.5	2090.10	−263	8		1.5	0.5	2319.00	975	−40
	0.5	0.5	2090.10	−75	15		−1.5	−0.5	2319.00	−1000	15
	−0.5	−0.5	2090.10	94	4		0.5	−0.5	2319.00	782	−29
	−1.5	−1.5	2090.10	291	20		−0.5	0.5	2319.00	−795	16
	−2.5	−2.5	2090.10	479	28		−0.5	−1.5	2319.00	577	−29
	−3.5	−3.5	2090.10	676	44		0.5	1.5	2319.00	−577	29
$R(3.5)$//	3.5	3.5	2626.80	−789	5		−1.5	−2.5	2319.00	385	−17
	2.5	2.5	2626.80	−554	13		1.5	2.5	2319.00	−385	17
	1.5	1.5	2626.80	−329	11		−2.5	−3.5	2319.00	205	8
	0.5	0.5	2626.80	−113	0		2.5	3.5	2319.00	−180	17
	−0.5	−0.5	2626.80	131	18						
	−1.5	−1.5	2626.80	357	17						
	−2.5	−2.5	2626.80	592	25						
	−3.5	−3.5	2626.80	827	33						

Rms = 41.80 MHz σ = 42.25 MHz

$$v = T_0 + B'J'(J'+1) - D'(J(J'+1))^2 - B''J''(J''+1) + D''(J''(J''+1))^2, \quad (1)$$

where T_0 is the band origin and B'/B'' and D'/D'' are the upper/lower state rotational and centrifugal distortion constants, respectively. The resulting molecular constants are listed in Table II. The constants for the [18.35]4.5-X(1)3.5 band are in good agreement with those reported in Ref. 2, within the stated experimental uncertainties.

Stark shift measurements and analysis

Stark shift measurements were carried out for the R(3.5) and Q(4.5) rotational lines of the [18.63]4.5-X(1)3.5(v'' = 0) transition and the R(3.5) line of the [18.35]4.5-X(1)3.5(v'' = 0) transition. Spectra were recorded with the laser polarization oriented either parallel (//) or perpendicular (⊥) to the applied field direction. These conditions impose the selection rules $\Delta M_J = 0$ or $\Delta M_J = \pm 1$, respectively (where M_J is the field-axis projection of the total angular momentum). The applied electric fields ranged from 1533 to 2319 V/cm. Representative spectra for the [18.63]4.5-X(1)3.5 R(3.5) line, for field-free conditions and a field of 2626.8 V/cm, are shown in Fig. 5.

The Stark Hamiltonian was defined by[15]

$$\hat{H}^{Stark} = -\boldsymbol{\mu_e} \cdot \boldsymbol{E} = -\mu_e E \cos(\theta), \quad (2)$$

where $\boldsymbol{E}$ is the electric field and $\boldsymbol{\mu_e}$ is the molecular electric dipole moment. For the low applied electric field strengths used in

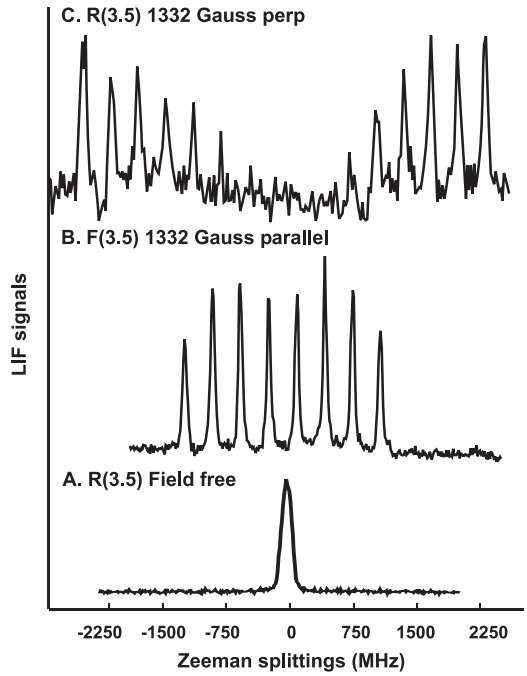

FIG. 6. Zeeman-effect spectra for the [18.63]4.5-X(1)3.5 R(3.5) rotational line. Trace A was recorded under field-free conditions. Traces B and C show the line splittings resulting from the application of a magnetic field of 1332 gauss.

these measurements, the Stark tuning of the degenerate Ω-doublet was adequately predicted by the first-order perturbation theory expression,[15]

$$\Delta\nu_{Stark}(\mathrm{MHz}) = \langle \Psi^{elec}; J\Omega M_J \pm |\hat{H}^{Stark}| \Psi^{elec}; J\Omega M_J \mp \rangle = \frac{-\mu_e E M_J \Omega}{J(J+1)} \times 0.503\,48, \quad (3)$$

where the electric dipole moment is in Debye units and E is the electric field strength in V/cm units. Note that the operator connects levels of opposite parity. A linear least-squares fitting program was used to analyze the data given in Tables III and IV. The Stark shifts of the two band systems were included in a simultaneous fit that yielded values for $|\mu_e|$ of 4.30(2), 4.05(3), and 4.32(2) D for the $X(1)3.5$, [18.35]4.5, and [18.63]4.5 states. The observed and calculated shifts are compared in Tables III and IV. The standard deviations for the fit were 20.0 and 42.3 MHz for the [18.35]4.5-$X(1)3.5$ and [18.63]4.5-$X(1)3.5$ band systems, respectively. These errors were commensurate with the estimated measurement uncertainty.

Zeeman shifts

Zeeman splittings were recorded for the R(3.5), R(4.5), Q(4.5), and Q(5.5) lines of the [18.63]4.5-$X(1)3.5$ transition and the R(3.5) and R(4.5) lines of the [18.35]4.5-$X(1)3.5$ transition. Magnetic fields of 470 and 1332 gauss were applied. Figure 6 shows the [18.63]4.5-$X(1)3.5$ R(3.5) line split by a magnetic field of 1332 gauss, with the laser polarization parallel and perpendicular to the field direction. The Zeeman splitting patterns were similar to those produced by the Stark effect, and the spectra were easily assigned. A total of 50 Zeeman shifts for the [18.35]4.5-$X(1)3.5$ lines and 104 shifts for the [18.63]4.5-$X(1)3.5$ lines were characterized. The data obtained from these measurements are collected in Tables V and VI.

The Zeeman Hamiltonian was taken to be[15]

$$\hat{H}^{Zeeman} = -\boldsymbol{\mu_m} \cdot \boldsymbol{B} = \mu_0 T^1(B) \cdot \left[\sum_i g_l T^1(l_i) + g_s T^1(s_i) \right], \quad (4)$$

where μ_0 is the Bohr magneton, $\boldsymbol{B}$ is the magnetic flux density, and g_l and g_s are the electronic orbital and spin g-factors. For both the [18.35]4.5-$X(1)3.5$ and [18.63]4.5-$X(1)3.5$ band systems, the magnetic moment associated with the rotation of the molecule could

TABLE V. Observed and calculated Zeeman shifts (MHz) for the UN [18.35]4.5-$X(1)3.5(v'' = 0)$ R(3.5) and R(4.5) lines.

Line, pol	M_J'	M_J''	Field (gauss)	Obs (MHz)	Obs-Calc (MHz)	Line, pol	M_J's	M_J''	Field (gauss)	Obs (MHz)	Obs-Calc (MHz)
$R(3.5)$//	3.5	3.5	1332	1564	30	$R(3.5)\perp$	4.5	3.5	1332	2844	−24
	2.5	2.5	1332	1105	9		3.5	2.5	1332	2414	−15
	1.5	1.5	1332	662	4		2.5	1.5	1332	1985	−6
	0.5	0.5	1332	216	−3		1.5	0.5	1332	1532	−21
	−0.5	−0.5	1332	−231	−12		0.5	−0.5	1332	1102	−12
	−1.5	−1.5	1332	−680	−22		−0.5	−1.5	1332	650	−26
	−2.5	−2.5	1332	−1112	−16		−1.5	−2.5	1332	220	−17
	−3.5	−3.5	1332	−1571	−37		−4.5	−3.5	1332	−2880	−12
$R(4.5)\perp$	5.5	4.5	1332	2485	−29		−3.5	−2.5	1332	−2410	19
	4.5	3.5	1332	2149	−12		−2.5	−1.5	1332	−1982	9
	3.5	2.5	1332	1794	−13		−1.5	−0.5	1332	−1575	−22
	2.5	1.5	1332	1443	−10		−0.5	0.5	1332	−1121	−7
	1.5	0.5	1332	1094	−6		0.5	1.5	1332	−688	−12
	0.5	−0.5	1332	765	19		1.5	2.5	1332	−223	14
	−0.5	−1.5	1332	396	3	$R(4.5)$//	4.5	4.5	1332	1578	−13
	−1.5	−2.5	1332	45	6		3.5	3.5	1332	1227	−10
	−2.5	−3.5	1332	−310	4		2.5	2.5	1332	877	−7
	−5.5	−4.5	1332	−2517	−3		1.5	1.5	1332	547	17
	−4.5	−3.5	1332	−2181	−20		0.5	0.5	1332	181	4
	−3.5	−2.5	1332	−1822	−15		−0.5	−0.5	1332	−168	9
	−2.5	−1.5	1332	−1479	−26		−1.5	−1.5	1332	−521	9
	−1.5	−0.5	1332	−1120	−20		−2.5	−2.5	1332	−874	10
	−0.5	0.5	1332	−766	−20		−3.5	−3.5	1332	−1224	13
	0.5	1.5	1332	−409	−16		−4.5	−4.5	1332	−1574	17
	1.5	2.5	1332	−54	−15						
	2.5	3.5	1332	338	24						

Rms = 16.32 MHz, σ = 16.83 MHz

TABLE VI. Observed and calculated Zeeman shifts in (MHz) for the UN [18.63]4.5-X(1)3.5(v'' = 0) R(3.5), R(4.5), Q(4.5), and Q(5.5) lines.

$R(3.5)$//	3.5	3.5	470	381	−21	$Q(5.5)$//	5.5	5.5	1332	2487	9
	2.5	2.5	470	286	−1		4.5	4.5	1332	2017	−10
	1.5	1.5	470	160	−12		3.5	3.5	1332	1566	−11
	0.5	0.5	470	62	5		2.5	2.5	1332	1096	−30
	−0.5	−0.5	470	−62	−5		1.5	1.5	1332	646	−30
	−1.5	−1.5	470	−165	7		0.5	0.5	1332	196	−29
	−2.5	−2.5	470	−278	9		−0.5	−0.5	1332	−235	−10
	−3.5	−3.5	470	−376	26		−1.5	−1.5	1332	−705	−29
$R(3.5)\perp$	4.5	3.5	470	815	−17		−2.5	−2.5	1332	−1137	−11
	3.5	2.5	470	704	−13		−3.5	−3.5	1332	−1606	−29
	2.5	1.5	470	585	−18		−4.5	−4.5	1332	−2056	−29
	1.5	0.5	470	482	−6		−5.5	−5.5	1332	−2506	−28
	0.5	−0.5	470	372	−1	$R(4.5)$//	4.5	4.5	1332	1256	17
	−0.5	−1.5	470	261	3		3.5	3.5	1332	978	15
	−1.5	−2.5	470	150	6		2.5	2.5	1332	690	2
	−2.5	−3.5	470	40	11		1.5	1.5	1332	412	−1
	−4.5	−3.5	470	−830	2		0.5	0.5	1332	144	6
	−3.5	−2.5	470	−720	−3		−0.5	−0.5	1332	−134	4
	−2.5	−1.5	470	−593	10		−1.5	−1.5	1332	−424	−11
	−1.5	−0.5	470	−490	−2		−2.5	−2.5	1332	−683	5
	−0.5	0.5	470	−380	−7		−3.5	−3.5	1332	−972	−9
	0.5	1.5	470	−269	−11		−4.5	−4.5	1332	−1252	−13
	1.5	2.5	470	−150	−6	$R(4.5)\perp$	5.5	4.5	1332	2063	−20
	2.5	3.5	470	−47	−18		4.5	3.5	1332	1788	−20
$R(3.5)$//	3.5	3.5	1332	1154	16		3.5	2.5	1332	1507	−26
	2.5	2.5	1332	826	13		2.5	1.5	1332	1277	19
	1.5	1.5	1332	488	0		1.5	0.5	1332	982	0
	0.5	0.5	1332	149	−14		0.5	−0.5	1332	707	0
	−0.5	−0.5	1332	−169	−6		−0.5	−1.5	1332	451	19
	−1.5	−1.5	1332	−498	−10		−1.5	−2.5	1332	177	20
	−2.5	−2.5	1332	−836	−23		−5.5	−4.5	1332	−2082	1
	−3.5	−3.5	1332	−1164	−26		−4.5	−3.5	1332	−1807	1
$R(3.5)\perp$	4.5	3.5	1332	2354	−5		−3.5	−2.5	1332	−1510	23
	3.5	2.5	1332	2021	−12		−2.5	−1.5	1332	−1257	1
	2.5	1.5	1332	1704	−4		−1.5	−0.5	1332	−982	0
	1.5	0.5	1332	1371	−12		−0.5	0.5	1332	−707	0
	0.5	−0.5	1332	1055	−3		0.5	1.5	1332	−451	−19
	−0.5	−1.5	1332	740	8		1.5	2.5	1332	−177	−20
	−1.5	−2.5	1332	409	2	$Q(4.5)$//	4.5	4.5	470	1006	−27
	−4.5	−3.5	1332	−2362	−3		3.5	3.5	470	784	−20
	−3.5	−2.5	1332	−2048	−15		2.5	2.5	470	555	−19
	−2.5	−1.5	1332	−1717	−9		1.5	1.5	470	339	−5
	−1.5	−0.5	1332	−1375	8		0.5	0.5	470	124	9
	−0.5	0.5	1332	−1066	−8		−0.5	−0.5	470	−124	−9
	0.5	1.5	1332	−750	−18		−1.5	−1.5	470	−339	5
	1.5	2.5	1332	−429	−22		−2.5	−2.5	470	−555	19
$Q(4.5)$//	4.5	4.5	1332	2941	13		−3.5	−3.5	470	−784	20
	3.5	3.5	1332	2295	18		−4.5	−4.5	470	−1006	27
	2.5	2.5	1332	1631	4						
	1.5	1.5	1332	980	4						
	0.5	0.5	1332	334	9						
	−0.5	−0.5	1332	−311	14						
	−1.5	−1.5	1332	−957	19						
	−2.5	−2.5	1332	−1660	−33						
	−3.5	−3.5	1332	−2255	22						
	−4.5	−4.5	1332	−2923	5						

Rms = 15.20 MHz, σ = 15.42 MHz

be neglected for the low applied magnetic fields used in these measurements. Analogous to the Stark effect, the tuning was adequately predicted by the first-order perturbation theory expression,[15]

$$\Delta\nu^{Zeeman} = \langle \Psi^{elec}; J\Omega M_J \pm |\hat{H}^{Zeeman}| \Psi^{elec}; J\Omega M_J \pm \rangle = \frac{-g_e \mu_0 B M_J \Omega}{J(J+1)}. \quad (5)$$

Note that the Zeeman operator connects levels of the same parity. In Eq. (5), g_e is the electronic expectation value of the operators in the square brackets in Eq. (4) and is used as the fitting parameter. The optimized g_e values obtained by least-squares fitting of the data are given in Table II. The standard deviations of these fits were 16.8 and 15.4 MHz for the [18.35]4.5-X(1)3.5 and [18.63]4.5- X(1)3.5 band systems, respectively.

Electronic structure calculations

Ab initio computational predictions for the ground and low-lying excited states of UN were presented in Refs. 4 and 5. These studies reported high-level calculations that included scalar relativistic effects, configuration interactions, and spin–orbit coupling. Large basis sets were employed, with extrapolation to the complete basis set limit. Both studies used small core 60-electron effective core potentials (ECP60) for U. The published results did not report values for the electric dipole moment of ground state UN. In a previous study of ThN,[16] it was found that BP86 density functional theory (DFT) calculations with a 60 electron ECP for Th yielded values for the ground state equilibrium distance, harmonic vibrational constant, and electric dipole moment that were in good agreement with the experimental values.

Consequently, in the present work, we have used the ORCA program package[17] to calculate the electric dipole moment and magnetic g_e-factor for ground state UN. The all-electron SARC-DKH-TZVP basis set (with SARC/J auxiliary functions) was used for U, in combination with the aug-cc-pVTZ basis for N. Scalar relativistic effects were included using the second-order Douglas–Kroll Hamiltonian. Spin–orbit coupling was treated using the Breit–Pauli Hamiltonian with treatment of both one- and two-electron terms as described in Ref. 18 and section 9.29.2 of the Orca manual for version 4.0.1. Evaluation of the matrix elements of the spin–orbit Hamiltonian employed semi-numeric calculations of the Coulomb terms, exchange via one-center exact integrals, and spin–other orbit interactions. Most calculations used the mean-field/effective potential approximation.[18]

Initially, the DFT/BP86 method was employed for spin-free calculations that were used to determine values for the equilibrium distance, vibrational constants, and dipole moment. To determine these properties, single-point calculations were carried out from R = 1.70 to 1.84 Å, in steps of 0.02 Å. These results were then fitted to a Morse potential. Calculations that included spin–orbit coupling were subsequently used to evaluate the g_e-factor at the equilibrium distance. The BP86 functional yielded spin-free properties that were in good agreement with the experimental values (R_e = 1.764 Å, ω_e = 1002 cm^{-1}, and μ = 4.37 D), but, with the inclusion of the spin–orbit coupling, the prediction of 1.27 for g_e was far from the observed value. As BP86 is a pure generalized gradient approximation method, we also carried out calculations using the B3LYP hybrid functional (20% Hartree–Fock exchange) and the range-separated version CAM-B3LYP. The results are collected in Table VII.

DISCUSSION

The magnetic g_e-value for the ground state of UN can be used to distinguish between different possible angular momentum coupling schemes and to evaluate previous predictions concerning the composition of the electronic wavefunction. The energy level pattern of UN is that of Hund's case (c) because of the large spin–orbit interaction. The only electronic quantum number that can be extracted from the analysis of an individual vibronic state is Ω. However, as illustrated in a study of the lanthanide monoxide CeO,[19] an interpretation of g_e can be particularly valuable in identifying normally unspecified, approximately good Hund's case (c) quantum numbers. As noted in the Introduction, the X(1)3.5 ground state wavefunction generated by *ab initio* calculations can be well represented by atomic ion basis functions arising predominantly from the $U^{3+}(5f^2 7s)N^{3-}$ configuration. Coupling between the spatially separated 5f and 7s orbitals is weak and best described by a j–j coupling scheme. The two interacting f-electrons couple to produce the sum of the orbital L_c, spin S_c, and total J_c electronic angular momenta for the $5f^2$ ionic core. The electronic angular momentum of the 7s electron, j, then couples with J_c to produce the total atomic ion angular momentum J_a. This electronic basis set is symbolically written as $\Psi^{elec} = |(((L_c S_c) J_c)(ls)\, j) J_a \Omega\rangle$. The expectation value of the spin and orbital angular momenta operators of Eq. (4) ($\equiv g_e$) was evaluated for this basis set in Ref. 19, and the resulting expression is reproduced here for convenience,

TABLE VII. Molecular Constants for UN X(1)3.5. Vibrational constants are in cm^{-1} units, electric dipoles are in Debye units, and the g_e values are dimensionless.

Method	ω_e	$\omega_e x_e$	Dipole	g_e	Reference
SO-CASPT2	1010	3	⋯	⋯	4
SO-CASPT2	1007	3	⋯	⋯	5
BP86	1003	3	4.37	1.27	This work
B3LYP	1211	20	3.65	2.07	This work
CAM-B3LYP	1064	3	4.61	1.22	This work
Experiment	1010.5(5.0)	4.2(2.5)	4.30(2)	2.16(1)	This work

$$g_e(L_c, S_c, J_c : l, s, j : J_a, \Omega) = (A + B)\frac{\Omega}{4J_a(J_a+1)},$$

where

$$A = \frac{J_a(J_a+1) + J_c(J_c+1) - j(j+1)}{J_c(J_c+1)}[3J_c(J_c+1) + S_c(S_c+1) - L_c(L_c+1)]$$

and

$$B = \frac{J_a(J_a+1) + j(j+1) - J_c(J_c+1)}{j(j+1)}[3j(j+1) + s(s+1) - l(l+1)]. \quad (6)$$

The quantum numbers for use in Eq. (6) are readily obtained using ligand field theory. Hund's rules predict that the $^3H_4$ term from the f^2 configuration will be lowest in energy and, thus, most relevant for the Ω = 3.5 ground state of UN. The *ab initio* calculations of Refs. 4 and 5 predict that the ΛS composition for the U^{3+} ion in the ground state of UN is ≥83% ^{4}H. Hence, the relevant quantum numbers for the basis set arising from the $U^{3+}(5f^2(^3H_4)7s)N^{3-}$ configuration are L_c = 5, S_c = 1, J_c = 4, l = 0, s = 0.5, j = 0.5, J_a = 3.5, and Ω = 3.5. Substitution into Eq. (6) gives g_e = 2.33. The remaining atomic ion character is distributed as 8% $^4\Gamma$ and 8% $^2\Gamma$, with g_e values of 3.25 and 3.11, respectively. The weighted sum predicts a g_e value of 2.47 for the $X(1)3.5$ ground state. The disagreement between this prediction and a measured value of 2.160 is not large enough to question the configurational parentage of the $X(1)3.5$ ground state, but it does suggest that the configuration interaction calculation has some deficiencies.

The ground state value for $\Delta G_{1/2}$ of 1010.5(5.0) cm^{-1} determined from the dispersed fluorescence data was consistent with the results obtained for UN trapped in a cryogenic Ar matrix. Green and Reedy[6] observed three bands in the 991–1001 cm^{-1} range that were assigned to UN. The splitting into three components was attributed to the presence of three distinct matrix trapping sites. Based on the response of the spectrum to annealing of the matrix, the band at 1000.9 cm^{-1} was considered to originate from UN at the most stable trapping site.[6] This frequency is just 9.6 cm^{-1} below the gas-phase value, which is entirely reasonable for the Ar matrix effect.

Recent computational predictions of the molecular constants for UN $X(1)3.5$ are compared to the experimental results in Table VII. Here, it can be seen that both *ab initio* (spin–orbit CASPT2[4,5]) and DFT methods yielded results that were in good agreement with the measured values. The previous computational studies did not report predictions for the electric dipole moment or the magnetic g_e-factor. Our DFT calculations yielded values for the electric dipole moment in the range of μ_e = 3.65 to 4.61 D at the equilibrium distance, in reasonable agreement with the measured value of μ_0 = 4.30 D. Comparing the ground states of UN and ThN, we find that the electric dipole moment of ThN [5.11(9) D] is larger than that of UN. The zero-point vibrationally averaged bond length for ThN (R_0 = 1.8222 Å) is slightly longer than that for UN (R_0 = 1.7641 Å), but this difference alone is not sufficient to account for the difference in the dipole moments. Considered in terms of the formal charge separation, $M^{\delta+}N^{\delta-}$, the charge difference for ThN (δ = 0.57) is greater than that for UN (δ = 0.51).

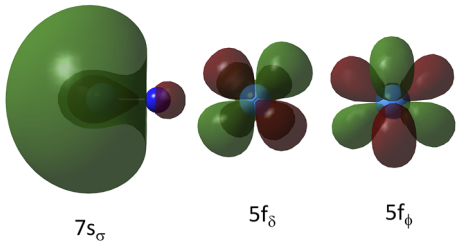

FIG. 7. The singly occupied frontier orbitals of the ground state UN. The 7s$_\sigma$ orbital is viewed along an axis that is perpendicular to the bond axis. The 5f$_\delta$ and 5f$_\phi$ orbitals are viewed along the bond axis in order to show the nodal planes. These orbitals are plotted on the same scale.

The model-dependence of the g_e values for ground state UN generated by the DFT calculations shows that the level of theory applied was insufficient for the recovery of this property. It is difficult to diagnose the root of this problem, but we note that the composition of the ΛS electronic wavefunction was, as expected, primarily $5f\ ^27s$. This is evident from the plots of the singly occupied orbitals shown in Fig. 7 (orbitals from the DFT/BP86 calculations). However, the Ω value for the spin–orbit coupled ground state was not defined. Note that changing how the electrons are distributed in the f-orbitals does not change the bonding significantly, so it is reasonable that the molecular constants and dipole moment would not be sensitive to f-orbital occupation details that markedly affect the g_e-factor.

The electric dipole moments obtained for the ground and excited states of UN were surprisingly similar. The most likely configurational assignments for the transitions reported here are that they are predominantly metal-centered $5f \rightarrow 6d$ or $7s \rightarrow 7p$ electron promotions.

SUMMARY

The electronic structure of UN has been examined using high-resolution spectroscopy of vibronic transitions centered at 18 349 and 18 630 cm^{-1}. External electric and magnetic fields were applied in order to measure electric dipole moments (from the Stark effect) and magnetic g_e-factors (from the Zeeman effect). The primary focus was on the properties of the ground state. Both the g_e-factor and the dipole moment were found to be consistent with previous studies that assigned the $X(1)3.5$ ground state to the formal $U^{3+}(5f^27s)N^{3-}$ electronic configuration. Dispersed fluorescence measurements defined ground state vibrational constants of ω_e = 1010.5(5.0) and $\omega_e x_e$ = 4.2(2.5) cm^{-1}. The first electronically excited state, (1)4.5, was observed just 471.5(5) cm^{-1} above the ground state. DFT calculations yielded a reasonably good prediction for the ground state dipole moment, equilibrium bond length, and harmonic vibrational constant. However, the ground state magnetic g_e-factor was greatly underestimated, indicative of problems with the details of the f-orbital occupations.

Electric dipole moment measurements for the excited states probed by direct laser excitation were close to the value obtained

for the ground state. This suggests that the transitions were electron promotions that resulted in relatively small changes in the polarizability of the metal ion.

ACKNOWLEDGMENTS

This material is based upon work supported by the U.S. Department of Energy, Office of Science, Office of Basic Energy Sciences, Heavy Element Chemistry program under Award No. DE-FG02-01ER15153. We are most grateful to Prof. Thomas Varberg (Macalester College) for his careful reading of the manuscript and recognition that the Ω-assignment of the 18 630 cm^{-1} band should be changed from 3.5 to 4.5.

AUTHOR DECLARATIONS

Conflict of Interest

The authors have no conflicts to disclose.

Author Contributions

Anh T. Le: Data curation (equal); Software (equal); Writing – review & editing (equal). **Xi-lin Bai**: Data curation (equal); Investigation (equal); Writing – review & editing (supporting). **Michael C. Heaven**: Formal analysis (equal); Funding acquisition (equal); Project administration (equal); Writing – original draft (equal); Writing – review & editing (equal). **Timothy C. Steimle**: Conceptualization (equal); Formal analysis (equal); Funding acquisition (equal); Investigation (equal); Project administration (equal); Supervision (equal); Writing – original draft (equal); Writing – review & editing (equal).

DATA AVAILABILITY

The data that support the findings of this study are available within the article.

REFERENCES

[1]V. Goncharov, L. A. Kaledin, and M. C. Heaven, J. Chem. Phys. **125**, 133202 (2006).
[2]D. J. Matthew and M. D. Morse, J. Chem. Phys. **138**, 184303 (2013).
[3]R. Tyagi, Z. Zhang, and R. M. Pitzer, J. Phys. Chem. A **118**, 11758 (2014).
[4]S. R. Battey, D. H. Bross, K. A. Peterson, T. D. Persinger, R. A. VanGundy, and M. C. Heaven, J. Chem. Phys. **152**, 094302 (2020).
[5]G. F. de Melo, M. Vasiliu, G. Liu, S. Ciborowski, Z. Zhu, M. Blankenhorn, R. Harris, C. Martinez-Martinez, M. Dipalo, K. A. Peterson, K. H. Bowen, and D. A. Dixon, J. Phys. Chem. A **126**, 7944 (2022).
[6]D. W. Green and G. T. Reedy, J. Chem. Phys. **65**, 2921 (1976).
[7]J. Han, A. T. Le, T. C. Steimle, and M. C. Heaven, J. Phys. Chem. Lett. **13**, 10799 (2022).
[8]M. C. Heaven, V. Goncharov, T. C. Steimle, T. Ma, and C. Linton, J. Chem. Phys. **125**, 204314 (2006).
[9]C. Linton, A. G. Adam, and T. C. Steimle, J. Chem. Phys. **140**, 214305 (2014).
[10]D. L. Kokkin, T. C. Steimle, and D. DeMille, Phys. Rev. A **90**, 062503 (2014).
[11]J. R. Gascooke, U. N. Alexander, and W. D. Lawrance, J. Chem. Phys. **134**, 184301 (2011).
[12]N. J. Reilly, T. W. Schmidt, and S. H. Kable, J. Phys. Chem. A **110**, 12355 (2006).
[13]H. Knoeckel, B. Bodermann, and E. Tiemann, Eur. Phys. J. D **28**, 199 (2004).
[14]C. M. Western, J. Quant. Spectrosc. Radiat. Transfer **186**, 221 (2017).
[15]J. M. Brown and A. Carrington, *Rotational Spectroscopy of Diatomic Molecules* (Cambridge University Press, 2003), p. 1046.
[16]A. T. Le, S. G. Nakhate, D.-T. Nguyen, T. C. Steimle, and M. C. Heaven, J. Chem. Phys. **150**, 144304 (2019).
[17]F. Neese, Wiley Interdiscip. Rev. Comput. Mol. Sci. **2**, 73 (2012).
[18]F. Neese, J. Chem. Phys. **122**, 034107 (2005).
[19]H. Schall, J. A. Gray, M. Dulick, and R. W. Field, J. Chem. Phys. **85**, 751 (1986).